Exciton-optical phonon coupling in II-VI semiconductor nanocrystals

Anne Myers Kelley

Chemistry & Chemical Biology, University of California, Merced

5300 North Lake Rd., Merced, CA 95343

amkelley@ucmerced.edu

Abstract

This Perspective reviews the topic of exciton-phonon coupling (EPC) in II-VI semiconductor nanocrystals. First, EPC is defined and its relevance is discussed, both as it influences the properties of the materials relevant to applications and as a probe of electronic structure. Different experimental and theoretical methods for probing EPC are outlined. Results for several different classes of II-VI nanocrystals are summarized. Finally, possible future directions are outlined.

Introduction

The Born-Oppenheimer approximation is the usual starting point for describing the spectroscopy of molecules. The nuclei are assumed to move slowly enough compared to the electrons that the electronic wavefunctions and energies may be calculated with the nuclei fixed in place. The equilibrium geometry is defined as the nuclear configuration at which the ground-state energy is a minimum. At this geometry the energies and wavefunctions of all of the excited electronic states of the system may, in principle, be calculated. The vibrational

wavefunctions of the electronic ground state are obtained in the harmonic approximation by expanding the ground electronic state energy as a Taylor series in the nuclear coordinates and truncating at quadratic terms. This constitutes the potential energy for nuclear motion in the harmonic limit. The set of coordinates in which the kinetic and potential energies for nuclear motion are simultaneously diagonal then defines the vibrational normal coordinates of the ground state.

If all electronic states of the molecule have the same dependence on nuclear coordinates, the energy separations between different electronic states are independent of nuclear coordinate. This is rarely the case. The simplest case is that the energy of each excited state differs from that of the ground state by a constant V_0 plus terms linear in one or more of the normal coordinates:

$$V_{ground} = \sum_k \hbar\omega_k q_k^2 \quad (1a)$$

$$V_{exc} = \sum_k \hbar\omega_k q_k^2 + g_k q_k + V_0 \quad (1b)$$

where q_k is a normal coordinate with frequency ω_k and linear exciton-phonon coupling constant g_k. Since adding a linear term to the potential energy does not change the second derivatives with respect to nuclear coordinates, the vibrational frequencies and normal modes of the excited state are unchanged from those of the ground state but the position of the potential minimum along one or more vibrational coordinates is changed (Figure 1) and the energy separations between different electronic states become a function of the nuclear coordinates. This is sometimes referred to as "vibronic coupling", but that term is more often reserved for situations in which not only the energy of the excited state but also its description is a function of nuclear coordinates. For example, displacement along a nuclear coordinate may mix different zero-order electronic wavefunctions (Herzberg-Teller coupling), allowing symmetry-forbidden electronic transitions to become allowed through excitation of a vibration of the correct symmetry. The situation where only the energies of the states depend on nuclear

coordinates is more specifically referred to as "Franck-Condon coupling" in chemistry, or "linear electron-phonon coupling" in physics.

The picture is essentially the same in nanocrystals but much of the language is different. The vibrational normal modes of a crystalline solid are usually referred to as phonons. The excited electronic states are called excitons if the excited electron and the "hole" (the set of orbitals from which the electron was promoted) are confined to the same region of the crystal. In a bulk crystal this occurs because of Coulombic interactions, while in a nanocrystal the physical size of the crystal may further limit the spatial extent of the exciton (quantum confinement). The dependence of the excitonic energies on phonon coordinate (*i.e.* Franck-Condon coupling) is then referred to as (linear) exciton-phonon coupling, or EPC. This is the focus of the current Perspective, although not all published studies are clear about what type of coupling is being addressed. The terms "exciton-phonon coupling" and "electron-phonon coupling" are often used interchangeably, but exciton is a more specific term for an electronic excitation that is spatially confined and overall charge neutral.

The vibrational frequencies and EPC magnitudes have several consequences for the spectroscopy and dynamics of nanocrystals. First, large EPC causes the intensity of a given excitonic transition to be distributed among many vibrational sublevels. This necessarily broadens the transition even if the sample can be made highly monodisperse in size and shape. This broadening is undesirable in applications that require a high transition strength over a narrow bandwidth such as nanocrystal lasers, displays that require color purity, or analytical sensors in which different labels are distinguished by their distinct emission spectra. The strength of EPC in phonons of various frequencies also enters into the rates of nonradiative processes including internal conversion, cooling of hot electrons and holes, and charge transfer across interfaces, all processes in which excess carrier energy is dissipated into phonons. In

order to optimize the rate or yield of a desired process it may be desirable to either minimize or maximize EPC. It follows that understanding EPC and how to control it synthetically is an important goal for enhancing many of the desired applications of semiconductor nanocrystals. Additionally, the ability to rationalize and predict EPC provides a good test of the fundamental understanding of both the phonons of semiconductor nanocrystals and their excitonic states.

Crystalline solids have two types of phonons, acoustic and optical. Acoustic phonons are those in which all of the atoms in a unit cell move with the same amplitude and direction, while optical phonons involve relative motions of the atoms within a unit cell. Optical phonons are further classified as longitudinal (the motions of the atoms are in the direction of propagation of the phonon) or transverse (the atomic motions are perpendicular to the propagation direction); the longitudinal optical (LO) phonons usually dominate the EPC in II-VI structures. Optical phonons usually occur at significantly higher frequencies than acoustic phonons and are therefore more accessible to frequency-domain spectroscopic techniques, while the acoustic phonons are more easily studied using time-domain techniques. This review is limited to EPC in optical phonons.

Experimental measurement of EPC

Many different experimental observables are sensitive to the magnitude of EPC in semiconductor nanocrystals, but most experiments provide only an indirect measurement of EPC. Extracting the EPC from the experimental data often requires modeling using assumptions and approximations that must be carefully chosen and validated.

The most direct way to measure EPC is to obtain a vibrationally resolved absorption or emission spectrum of a cold sample. If the initial population is almost entirely in the $v = 0$ phonon level, then the intensity of the $0 \rightarrow v$ transition relative to that of the origin transition (0

$\rightarrow 0$) for linear EPC is given by the Poisson distribution, $\frac{I(v)}{I(0)} = e^{-S}\frac{S^v}{v!}$ where S is the Huang-Rhys parameter; $S = \frac{\Delta^2}{2}$ where Δ is the displacement between the potential energy minima of the ground and excited states in units of the dimensionless phonon coordinate (Figure 1). Note that the Huang-Rhys parameter is proportional to the integrated intensity of the transition, so peak areas rather than peak heights should be used for determining it from experimental data; the bandwidths tend to increase for higher v because of faster vibrational dephasing. For a simple diatomic stretching coordinate, $\Delta = \sqrt{\frac{\mu\omega}{\hbar}}\delta r$ where μ is the reduced mass, ω is the vibrational frequency, and δr is the difference between ground and excited state equilibrium bond lengths; for a normal mode of a polyatomic system, μ and δr have more complicated definitions. $\Delta = 1$ means that the equilibrium geometries differ by an amount corresponding to the zero-point displacement of the ground-state vibrational probability distribution.

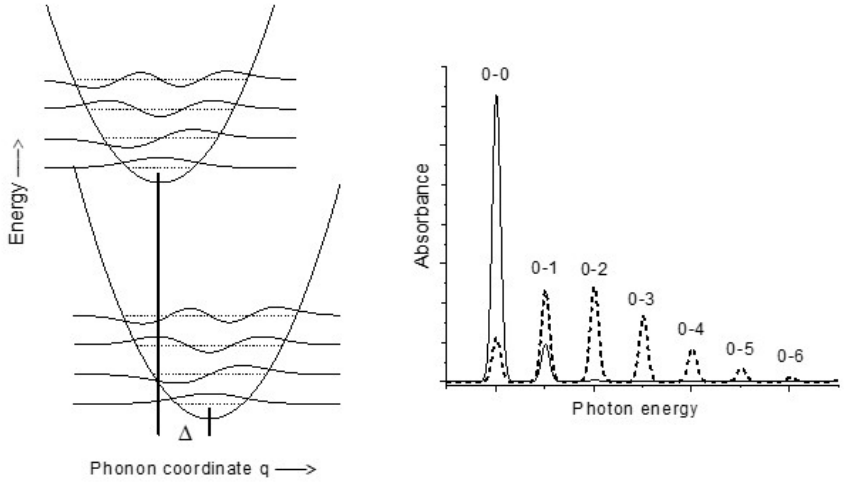

Figure 1. Left: Potential energy curves and vibrational wavefunctions for ground and excited electronic states along a phonon coordinate with linear exciton-phonon coupling. Right: Absorption spectra corresponding to Δ = 0.5 (S = 0.125), solid, and to Δ = 2.0 (S = 2.0), dashed.

The optical phonon frequencies of most II-VI semiconductors are in the 150-350 cm^{-1} range. Even relatively monodisperse ensembles typically have optical inhomogeneous linewidths somewhat greater than this. Therefore, if the goal is to produce samples that emit with high spectral purity for applications in quantum dot lasers, displays, or optical sensors, variations in S in the range from 0 (all intensity in the origin transition) to 0.5 (39% of the intensity in $v > 0$ transitions) have little effect, but $S > 1$ would cause significant broadening of the transition. On the other hand, large values of S are desirable to enhance the rates of nonradiative processes that require converting significant amounts of electronic energy into phonon energy.

It is straightforward to extract the EPC in each phonon mode from the type of spectrum shown in Figure 1; the problem is that it is rarely possible to get the spectrum. Even the most monodisperse samples of nanocrystals contain enough heterogeneity in size, shape, ligand coverage, *etc*. to largely wash out the phonon substructure. A vibrationally resolved spectrum can be obtained only by going to very low temperatures and probing single nanocrystals[4-5] or exciting on the extreme red edge of the ensemble-broadened absorption spectrum (emission line-narrowing) to observe the spectrum of a small subensemble.[6-7] Single-nanocrystal experiments tend to select for those members of the ensemble that are particularly bright and resistant to photobleaching or blinking and may not be representative of the sample as a whole. Furthermore, obtaining a spectrum of a single nanocrystal necessarily requires that the nanocrystal absorb many photons in a short period of time, making these spectra susceptible to light-induced changes to the sample. Emission line narrowing works only at very low temperatures, such that no hot bands contribute to the absorption and the position of a given absorber within the inhomogeneous distribution does not fluctuate in time, and it can probe only that subset of the ensemble that absorbs at the longest wavelengths and is thus not very representative of the whole.

Absorption or emission spectra of ensembles sometimes exhibit hints of phonon substructure even at room temperature. This is particularly true of nanoplatelets, in which inhomogeneous broadening is greatly suppressed. The overall width of the absorption or emission spectrum also allows some limits to be placed on the EPC strength. However, attempting to extract quantitative Huang-Rhys parameters from vaguely structured spectra is fraught with uncertainties surrounding the frequencies of the coupled phonons and the contributions to the width from inhomogeneous broadening and multiple excitonic states.

Spectroscopic measurements of EPC on ensembles usually rely on multiphoton techniques, chiefly resonance Raman[1-3, 8-20] and its time-domain analogs.[21-30] In a resonance Raman process an incident photon is destroyed and a scattered photon is created, leaving the system in a state that differs from that of the initial state by one or more phonons. The process is described quantum mechanically by using second-order time-dependent perturbation theory to calculate the probability of making a transition from the initial state to the final state *via* all possible excited intermediate states. The Raman amplitude, whose absolute square is proportional to the Raman scattering cross-section, may be calculated either in the frequency domain or in an equivalent time-domain formulation which more clearly demonstrates the role of EPC in the scattering process (Figure 2). Other things being equal, as the EPC in a particular phonon mode is increased, the resonance Raman scattering into that mode becomes stronger and in particular the overtones (transitions in which the number of vibrational quanta changes by more than one) become stronger. In this type of experiment the time dependence is only inferred; the actual measurement is performed in the steady state.

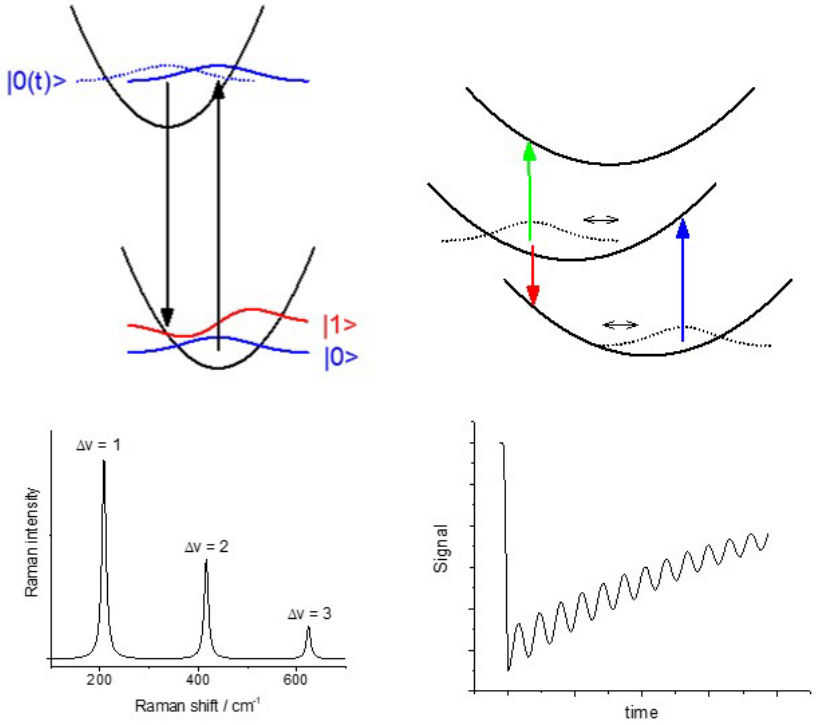

Figure 2. Left: Time-dependent wavepacket picture of resonance Raman scattering. Interaction with the laser field projects the initial wavefunction $|0\rangle$ onto the excited-state potential surface, where it becomes a moving wavepacket, $|0(t)\rangle$. Fourier transformation of the overlap $\langle n|0(t)\rangle$ gives the Raman excitation profile for the $\Delta v = n$ transition, from which the Raman spectrum can be obtained. Right: Pump-probe spectroscopy. Interaction with a short laser pulse generates moving wavepackets on both the ground- and excited-state surfaces. The transmission of a delayed probe pulse has contributions from ground-state bleaching (blue arrow), excited-state absorption (green), and stimulated emission (red), all of which are modulated by the wavepacket motion. Other time-domain signals such as photon echoes are similarly modulated.

In a pump-probe experiment a laser pulse that is short compared to the phonon frequencies of interest, and therefore necessarily spectrally broad, excites the sample, setting up a coherence among multiple vibrational levels that can be interpreted as a classical-like oscillatory motion of the nuclei. The transmittance of a short probe pulse arriving a variable time later will then be modulated by this impulsive nuclear motion; the larger the EPC, the greater the depth of modulation (see also Figure 2). Two-pulse pump-probe measurements of this type, when the pump and probe are both electronically resonant, are usually referred to as transient absorption or, when the emphasis is on the vibrational coherences, as (resonant) impulsive stimulated

Raman scattering.[31] Other time-domain methods such as photon echoes involve more independently manipulated pulses but rely on the same general idea of setting up a vibrational coherence that modulates the signal produced by a variably delayed probe pulse. While the time-domain approaches are sometimes claimed to provide a more direct measurement of EPC with fewer possible artifacts, both types of techniques have many experimental pitfalls. Analysis of both types of data requires consideration of all of the possibly overlapping excitonic states, the different EPCs for each of the phonon modes, and the magnitudes of homogeneous and inhomogeneous spectral broadening. Time-domain experiments additionally require an accurate spectral and temporal description of the pump and probe pulses.

There are some other experimental measurements through which EPC strengths may be inferred. The temperature dependence of the absorption or emission bandwidth is determined in part by EPC but also by a number of other factors that are difficult to disentangle.[32] Resonances in electron tunneling spectroscopy have also been found to exhibit phonon progressions from which the coupling of the phonons to the conduction band electron can be obtained.[33-34]

Calculation of EPC

Calculation of EPC strengths for any finite-sized collection of atoms, be it a semiconductor nanocrystal or a molecule, is straightforward in principle. The minimum-energy nuclear geometry is first calculated for the ground state of the system. All of the second derivatives of the potential energy for nuclear motion with respect to the nuclear coordinates are then calculated at the ground-state equilibrium geometry, and from that, along with the masses of the atoms, the harmonic vibrational normal modes of the system are obtained. The minimum-energy nuclear geometry for the desired electronically excited state is then calculated and the

excited state to ground state geometry difference is projected onto each ground-state normal mode.[35-36] This procedure yields the EPC for each ground-state mode in the limit of linear electron-phonon coupling. The accuracy of this procedure depends largely on the method used to calculate the ground- and excited-state wavefunctions, including any solvent or environmental effects, and on the appropriateness of assuming harmonic vibrations and linear electron-phonon coupling.

This approach is difficult to apply to semiconductor nanocrystals because of the size of the systems involved, typically hundreds to thousands of heavy atoms. High quality electronic structure calculations even for the ground state are slow and expensive particularly when ligands are included or when multiple structures need to be calculated to account for the polydispersity of real experimental systems. While density functional theory calculations of EPC have been reported for some structures of the size commonly studied in experiments,[35] usually the ground-state equilibrium geometry and force constants needed to determine the phonon modes are obtained by using empirical force fields parameterized through comparison with experiment and, in some cases, electronic structure theory.[37-38] The excitonic wavefunctions are modeled as the electron and hole functions calculated from an effective mass approximation using a confining potential of appropriate size and shape, with varying degrees of sophistication.[36]

EPC in semiconductor nanocrystals is usually partitioned into two contributions, the deformation potential coupling and the Fröhlich coupling. The deformation potential refers to the changes in chemical bonding that occur upon excitation and cause the equilibrium positions of the atoms to change, while the Fröhlich coupling refers to the forces imposed on the charged atoms (ions) in the lattice by the electric fields set up by different spatial distributions of electron and hole. The deformation potential coupling corresponds most closely to the

normally envisioned mechanisms for EPC in molecules. The Fröhlich coupling, which requires at least partially ionic bonding and is operative over longer distances, is usually assumed dominant for the optical phonons of polar semiconductors such as CdSe and other II-VI compounds. Electronic structure calculations based on atom-centered orbitals capture both effects.

Experimental results for EPC in semiconductor nanocrystals

As the literature on EPC in semiconductor nanocrystals is vast, this discussion is limited to experimental results for optical phonons in II-VI nanocrystals in which the materials are reasonably well defined and quantitative values for the Huang-Rhys parameter are either reported or can be estimated from the data presented.

Our group has approached the determination of EPC strengths in semiconductor nanocrystals through quantitative resonance Raman spectroscopy.[1-2, 8-9, 20] In these studies, resonance Raman spectra are obtained at several resonant excitation wavelengths and the absolute Raman scattering cross-sections for the LO phonon and its overtones are obtained by ratioing the integrated Raman intensities of the nanocrystal to that of a solvent whose absolute Raman cross-section is known. The Raman intensities and the optical absorption spectrum are then simulated using a common model that includes the energies and transition dipole moments of the various resonant excited states, the Huang-Rhys parameters for the phonons, and the homogeneous and inhomogeneous linewidths of the excitonic states. See, for example, Table I of ref. 8 and Table 1 of ref. 1. This approach takes advantage of the fact that the absorption spectrum, while it is relatively unstructured, can be measured with high accuracy and depends on the same physical parameters as the resonance Raman profiles, so any model for the Raman intensities must also be consistent with the absorption spectrum.

Our approach is closely related to the pioneering early work of the Alivisatos group on CdSe and CdS nanocrystals,[12-13] although the available synthetic methods at the time produced lower quality samples and they were too early to take advantage of the work of the Bawendi and Efros groups in locating the overlapping excitonic transitions and elucidating the excitonic fine structure.[39-40] Most other recent studies of EPC using resonance Raman spectroscopy analyze the data using highly simplified versions of the resonance Raman cross-section expression that omit multiple overlapping excitonic states and inhomogeneous broadening, often use unrealistic values for the homogeneous width, and are not consistent with the absorption spectra of the samples studied. In some cases the Huang-Rhys parameter is simply assumed equal to the ratio of the first overtone to fundamental integrated Raman band intensities; in a direct absorption or emission spectrum this ratio is actually given by S/2, but considerable deviations are possible in a resonance Raman process because of the interferences among intermediate states.[11] Pump-probe and photon echo experiments, in which the coupled phonons are observed directly as oscillations in the time domain, are also usually analyzed with simple models that assume a single resonant excitonic state and do not treat the broadening in a manner that is consistent with the optical spectra. The assumption of a single resonant excitonic state can be particularly problematic in time-domain studies where the pulses used are often spectrally very broad.

Single-component quantum dots

A variety of studies have probed exciton-phonon coupling in single-component CdSe quantum dots having only organic ligands on the surface. Our group carried out resonance Raman studies as a function of excitation energy for several different sizes.[1, 8] While our first set of experiments yielded a best-fit Huang-Rhys parameter of about 0.10 for the LO phonon in the

two lowest excitonic transitions, later work was more consistent with values in the 0.18-0.24 range. Notably, the Huang-Rhys parameter associated with the lowest-energy excitonic transition was found to be nearly independent of QD diameter from 2.6 to 5.2 nm. The early work of Alivisatos,[12] on samples that were about 4.5 nm in diameter but quite polydisperse, yielded a similar Huang-Rhys parameter of 0.25. Mittleman *et al.* performed three-pulse photon echo experiments on CdSe QDs from 2.1 to 4.0 nm diameter and fit the oscillatory decays to a model containing vibrational oscillations and dephasing.[21] They obtained S = 0.13 to 0.25, slightly increasing with increasing QD size. Salvador and Scholes also carried out three-pulse photon echo measurements on CdSe QDs from 3.0 to 4.0 nm diameter and obtained coupling strengths corresponding to S = 0.05 to 0.15, with no consistent dependence on size.[23-24] Kambhampati's group analyzed the femtosecond pump-probe signals from CdSe QDs between 3.1 and 5.4 nm diameter and found very small Huang-Rhys parameters for the LO phonon, $S \leq 0.025$, increasing slightly for larger sizes and decreasing for higher-energy excitons.[25-26] They also stated that a much larger Huang-Rhys parameter of $S \sim 4.5$ was required to reproduce their steady-state resonance Raman spectra, but that S value appears inconsistent with the modest overtone intensities measured. Our group in collaboration with Kambhampati's analyzed chirped pulse femtosecond pump-probe signals from 4.0 nm diameter CdSe QDs and obtained a best-fit value of S = 0.24 for the LO phonon, pumping and probing on the low-energy side of the lowest exciton transition.[29] Groeneveld and Donega obtained vibrationally resolved emission spectra of CdSe QD ensembles at low temperature by exciting near the red edge of the absorption spectrum, thus selecting only the reddest-absorbing members of the ensemble.[6] They obtained S = 0.8 - 1.0 from the $\Delta v = 1$ to $\Delta v = 2$ intensity ratios.

Two other measurements of phonon coupling in CdSe QDs are not directly comparable to those discussed above. Shim and Guyot-Sionnest carried out intraband spectral hole burning of

the $1S_e$-$1P_e$ transition of 3 - 5 nm diameter CdSe QDs in a low-temperature glass.[41] From the intensities of the phonon sidebands they deduced a Huang-Rhys parameter of S = 0.13 – 0.2, increasing with decreasing size. Note that this value is for a transition between two different conduction-band states of the electron and includes no contribution from the hole, and is not directly related to the Huang-Rhys parameter for an excitonic transition between the ground state and an electron-hole pair state. Sun *et al.* carried out low-temperature scanning tunneling microscopy (STM) on single CdSe QDs and resolved a progression with an energy spacing corresponding to the LO phonon.[33] From the intensities of the peaks they obtained a Huang-Rhys parameter of 0.35. This refers to transitions of an extra conduction band electron in a negatively charged QD, and again is not directly comparable to the Huang-Rhys parameter for creation of an exciton.

Other single-component quantum dots have been studied less extensively. Our group measured and modeled the resonance Raman intensities of 3.8 - 4.9 nm diameter ZnSe QDs and obtained Huang-Rhys parameters of S = 0.3 - 0.5.[9] The Alivisatos group carried out a resonance Raman study of CdS QDs ranging from 0.9 – 6.4 nm, measuring both overtone to fundamental ratios and absolute scattering cross-sections and modeling the data to find the best-fit value of the Huang-Rhys parameter.[13] They found a strong size dependence, with S ranging from less than 0.1 for the smallest particles to greater than 1.0 for the largest ones. Krauss and Wise studied EPC in PbS QDs using both resonance Raman spectroscopy and three-pulse photon echoes.[14, 22, 30] They found S ~ 0.7 based on the Raman data but S ~ 0.01 from the time-domain measurements, and concluded that the steady-state (Raman) measurements greatly overestimate the true Huang-Rhys parameter by generating trapped surface charges that produce strong local electric fields. (Note that lead chalcogenides have the rocksalt crystal structure in which fundamental Raman scattering is forbidden, and it is not clear whether the

apparent LO phonon fundamentals arise from symmetry breaking in the nanocrystal or from products of photooxidation.)[42-43] Electron tunneling spectroscopy on PbS QDs revealed phonon progressions that were fit to S ~ 1.7 - 2.5.[34] Dimitrov *et al*. carried out femtosecond pump-probe measurements on CdTe QDs and fit the oscillatory decays to obtain values of S = 0.013 ± 0.006 over a range of particle sizes.[27] Zhang *et al*. measured the UV resonance Raman spectra of ZnO QDs in the 8.5-11.5 nm size range, in the very weak quantum confinement limit.[18] They studied both neutral QDs and those that had been photocharged to produce free electrons in the conduction band, and they modeled the overtone to fundamental intensity ratio using a single-state model with different assumptions about the linewidth. They found Huang-Rhys parameters of roughly 2.0 - 2.2 for the neutral QDs and 1.0 - 1.5 for the photocharged ones.

Nanorods

Lange *et al*. used Raman spectroscopy at low temperature to explore EPC in CdSe nanorods.[16-17] They measured the LO overtone to fundamental ratios but modeled the data using an unreasonably small homogeneous linewidth and no inhomogeneous broadening, yielding S = 0.05 - 0.02.

Nanoplatelets

Nanoplatelets are an interesting class of nanocrystals that are relatively large in two dimensions and have a well-defined thickness of just a few layers in the third dimension. Because the quantum confinement is almost entirely in the thickness dimension and is essentially identical for all members of the ensemble, there is very little inhomogeneous broadening and the absorption and emission spectra are quite sharp. Simple modeling of the band shape of the lowest-energy excitonic transition confirms that the Huang-Rhys parameter

for the optical phonon cannot exceed S ~ 0.5. A couple of studies have further refined this value. Achtstein *et al*. measured single-nanoplatelet emission spectra of 5.5 monolayer structures and found S = 0.059 for the LO phonon, in good agreement with the value inferred from the temperature dependent width of the emission spectrum.[4] Our group measured resonance Raman spectra and absolute cross-sections for 4.5 monolayer structures and modeled the Raman and absorption spectra, obtaining a Huang-Rhys parameter of 0.08 on resonance with the lowest-energy transition.[20]

Core/shell structures

Exciton-phonon coupling has also been studied in core/shell structures. Most of these are "type I" structures such as CdSe/ZnS, in which both the electron and the hole are energetically favored to be localized in the core. There has also been some work on "type $I^{1/2}$" or "quasi-type II" structures such as CdSe/CdS, in which the hole is localized in the core but the electron is significantly delocalized between core and shell. Few studies have addressed "type II" materials in which the electron and the hole are energetically favored to reside in different materials and creation of the lowest-energy exciton therefore corresponds to charge transfer between core and shell.

Baranov *et al*. measured the resonance Raman overtone to fundamental intensity ratios of type I CdSe/ZnS core/shells and obtained S ~ 0.2 over a range of shell thicknesses.[15] Valerini *et al*. studied the temperature dependence of the emission linewidth in CdSe/ZnS core/shell QDs in a polystyrene matrix and fit the data to a model that contains broadening from both acoustic and optical phonons.[32] The optical EPC was found to be Γ_{LO} = 21 meV; applying the conversion from ref. 4 that $\Gamma_{LO} = S^{1/2} E_{LO}$, we obtain S = 0.7 for the CdSe/ZnS QDs. Fernee *et al*. measured low-temperature single-particle photoluminescence from CdSe/CdZnS QDs.[5] They found that

considerable variability in the emission spectra of different QDs, but most showed a resolved LO phonon feature with an intensity suggesting a Huang-Rhys parameter ranging from near zero to ~0.4. Salvador *et al.* found from three-pulse photon echo measurements that adding a ZnS shell to a CdSe core hardly affected the Huang-Rhys parameter for the LO phonon (S = 0.10-0.12).[23] McKimmie *et al*. carried out three-pulse photon echo measurements on CdSe QDs capped with CdS, CdS/ZnS, and CdS/CdZnS/ZnS shells.[28] They fit the oscillatory decays to a model containing both Gaussian and exponential dephasing as well as acoustic and optical phonons, resulting in a Huang-Rhys parameter for the optical phonon of S ~ 0.2 for all three samples.

Our group used resonance Raman intensity analysis to probe the effect of adding a quasi-type II CdS shell to CdSe cores.[2] The expectation was that delocalization of the electron wavefunction into the CdS shell would produce more change separation and therefore stronger EPC for the CdSe phonons via the Fröhlich mechanism. However, the Huang-Rhys parameter for the CdSe LO phonon in the lowest excitonic transition was found to be only about 0.13 for either thin or thick shells, somewhat smaller than for bare CdSe cores. Groeneveld and Donega extended the fluorescence line-narrowing experiments mentioned above to quasi-type II and type II CdTe/CdSe core/shell structures.[6] They obtained S values of 1.5 and 2.9, respectively, consistent with the expectation that increasing charge separation increases EPC.

These experimental results are summarized in Table 1. There is a reasonable consensus that the average Huang-Rhys parameter for the LO phonon of CdSe QDs, with or without a semiconductor shell, falls in the range S = 0.1 – 0.3. It is smaller for nanoplatelets and there are inadequate data on nanorods. Data on other semiconductors are too sparse to allow any conclusions to be reached.

Table 1. Experimentally determined Huang-Rhys parameter (S) for the longitudinal optical phonons of II-VI semiconductor nanocrystals, lowest excitonic transition unless otherwise stated.

material	shape	size	shell	method	S	comments	ref.
CdSe	dot	3.2 nm diam	none	Raman	0.10	higher and lower values found in higher states	8
CdSe	dot	4.0 nm diam	none	fs pump-probe	0.24		29
CdSe	dot	2.6 – 5.2 nm diam	none	Raman	0.24 – 0.18	higher and lower values found in higher states	1
CdSe	dot	4.5 nm diam	none	Raman	0.25		12
CdSe	dot	2.1 – 4.0 nm diam	none	3-pulse photon echo	0.13 – 0.25		21
CdSe	dot	3.0 – 4.0 nm diam	none	3-pulse photon echo	0.15 – 0.05		24
CdSe	dot	4.0 nm diam	none	3-pulse photon echo	0.10 – 0.12		23
CdSe	dot	5.6 nm diam	none	fs pump-probe	0.025	lower values found in higher states	26
CdSe	dot	3.2 – 5.4 nm diam	none	fs pump-probe	0.02 – 0.03		25
CdSe	dot	3.0 – 4.3 nm diam	none	line-narrowed emission	0.8 – 1.0		6
CdSe	dot	3 – 5 nm diam	none	spectral hole burning	0.13 – 0.20	intraband transition of conduction electrons	41
CdSe	dot	6 nm diam	none	low-temp STM	0.35	intraband transition of excess conduction band electrons	33
CdSe	rod	3.5 nm diam, aspect ratio ~2	none	low-temp STM	0.62	intraband transition of excess conduction band electrons	33

CdSe	rod	3 – 8 nm diam, 25 – 80 nm long	none	Raman	0.02 – 0.05	fixed excitation above lowest exciton	17
CdSe	nano-platelet	4.5 ML thick	none	Raman	0.08		20
CdSe	nano-platelet	5.5 ML thick	none	single-particle emission	0.059		4
CdSe	dot	4.0 nm diam	0.5 – 3.4 ML ZnS	Raman	0.2	fixed excitation above lowest exciton	15
CdSe	dot	5.0 nm diam	ZnS	temp-dep emission linewidth	0.7		32
CdSe	dot	3 – 5 nm diam	CdZnS	single-particle emission	~0 - ~0.4	HR param estimated from spectra	5
CdSe	dot	4.0 nm diam	ZnS	3-pulse photon echo	0.10 – 0.12		23
CdSe	dot	4 nm diam	CdS, CdS-CdZnS-ZnS, CdS-ZnS	3-pulse photon echo	~0.2		28
CdSe	dot	2.7 nm diam	0.5-1.6 nm CdS	Raman	0.125		2
ZnSe	dot	3.8 – 4.9 nm diam	none	Raman	0.3 – 0.5		9
CdS	dot	0.9 – 6.4 nm diam	none	Raman	<0.1 - >1.0	increasing HR param with increasing size	13
PbS	dot	3.0 nm diam	none	Raman	0.7		14
PbS	dot	3.0 nm diam	none	3-pulse photon echo	0.01		30
PbS	dot	6 – 9 nm diam	none	electron tunneling spectroscopy	1.7 – 2.5		34
ZnO	dot	8.5 – 11.5 nm diam	none	Raman	2.0 – 2.2	very weak quantum confinement	18
ZnO	dot	8.5 – 11.5 nm diam	none	Raman	1.0 – 1.5	photocharged, excess electrons	18

CdTe	dot	2.5 – 3.5 nm diam	none	femtosecond pump-probe	0.013 ± 0.006		27
CdTe	prolate dot	4.4 nm long	CdSe quasi-type II	line-narrowed emission	1.5	includes LO phonons of both core and shell	6
CdTe	bipod	8 nm long	CdSe type II	line-narrowed emission	2.9	includes LO phonons of both core and shell	6

Discussion

The exciton-phonon coupling strength depends on both the nature of the phonon mode (the amplitudes and directions of motion of each of the atoms) and the changes in the charge distributions between the ground state and the excited excitonic state. It is different for each phonon mode in each excitonic state,[36, 44] although it often makes sense to discuss the total EPC in all optical phonons in a given excitonic state and this is implicitly done in most studies that report the "EPC for optical phonons". In molecules, the descriptions and approximate frequencies of the vibrational normal modes can usually be obtained with fair accuracy from either an empirical force field calculation or an electronic structure theory calculation on the ground state, and the excited states are often described reasonably well as an excitation of an electron from the highest occupied molecular orbital (HOMO) to the lowest unoccupied orbital (LUMO). From an approximate description of those two orbitals, corresponding to the top of the valence band and the bottom of the conduction band in semiconductor crystals, one can usually determine qualitatively how the equilibrium geometry will change upon excitation, and therefore which vibrational modes will undergo the strongest coupling.[45]

Transferring these ideas to semiconductor nanocrystals is complicated by several factors arising from the quasiperiodicity of the structure and the bulk-like models typically used to describe the electronic excitations. The phonon modes of a bulk crystal are described as a set of

atomic motions at the unit cell level multiplied by an envelope function that gives the amplitude and phase of the contribution of each unit cell. A unit cell consisting of N atoms has three acoustic modes and 3N-3 optical modes, and once the optical modes are determined at the unit cell level, the extended phonons of an infinite perfect crystal are completely defined by their wavevectors. The phonon confinement model describes the phonons of a nanocrystal as linear combinations of the bulk phonons with coefficients chosen to obey the boundary conditions at the edges of the nanocrystal. However, real nanocrystals often have incomplete unit cells at their edges and the equilibrium geometries and force constants for the surface atoms are somewhat different from those of the bulk materials. The ligands on the surface atoms further influence the phonons. Because any factor that breaks the degeneracy among different local oscillators is likely to result in localization of the wavefunctions, we expect that the phonon modes of a nanocrystal will be more localized than those of a corresponding sized piece of a bulk crystal. Our group has investigated this using empirical force fields for CdSe quantum dots and has found that different force fields predict significantly different extents of disorder in the crystal structure and extents of localization of the phonons.[37] Thus, while we may have a very good description of the longitudinal optical phonon at the unit cell level, we lack a clear picture of what the various LO phonons look like across the whole nanocrystal.

Under the assumption of purely Fröhlich type coupling, EPC will exist only to the extent that the spatial distributions of the electron and the hole are different, thus creating local electric fields that can couple to the polar optical phonons. The usual picture is that in a bulk polar semiconductor the electron and hole are Coulombically bound, with the electron occupying a much larger volume owing to its smaller effective mass. Excitons in bulk semiconductors should therefore produce large local electric fields that can couple strongly to polar phonons of appropriate symmetry. As the bulk crystal is reduced in size below the Bohr radius, the

electron becomes confined to a volume more similar to that of the hole and the EPC is reduced. Further reducing the size of the nanocrystal causes the electron to start tunneling out of the nanocrystal into the classically forbidden region, while the hole, with its greater effective mass, remains confined to the interior of the nanocrystal. This increases the extent of charge separation again and increases the EPC (Figure 3). We expect, therefore, that the EPC should show a minimum at a size somewhat smaller than the Bohr radius for the free exciton. However, this is almost never observed in experiments; often almost no size dependence is observed, and there is no clear pattern in those experiments that do observe a size dependence.

Our group found almost no dependence of the LO EPC on size for CdSe QDs over a factor of two variation in diameter (Figure 3).[1] Furthermore, adding a CdS shell, which should have increased the EPC by increasing the extent of charge separation in the exciton, had the opposite effect (Figure 3).[2] This led us to suggest that the electron and/or hole wavefunction, most likely the latter, is far more localized than simple particle-in-a-sphere effective mass approximation models would predict, likely because of the presence of defects or charges on the surface that

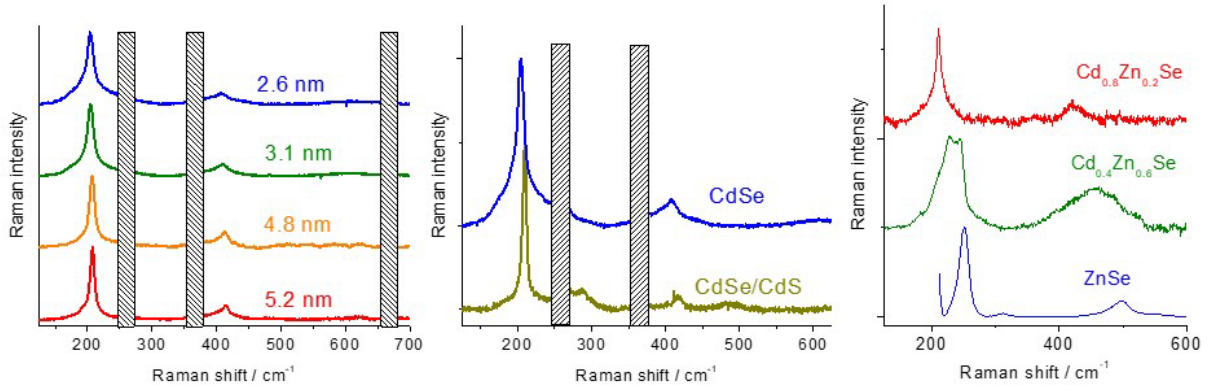

Figure 3. Resonance Raman spectra excited near the lowest excitonic maximum in each case; bars block solvent peaks. Left: CdSe QDs of different diameters. The LO phonon overtone (near 400 cm^{-1}) to fundamental (near 200 cm^{-1}) intensity ratios are nearly independent of size. Data from ref. 1. Middle: CdSe QDs with and without a CdS shell. The CdSe LO phonon overtone to fundamental ratio is greater for the bare CdSe. Data from ref. 2. Right: ZnSe and ZnSe/CdSe alloyed QDs. The overtone (400-500 cm^{-1}) to fundamental (200-250 cm^{-1}) intensity ratio is greatest for intermediate compositions. Data from ref. 3.

are partially removed by adding a shell. (Charges on the outer shell surface have little effect on the hole wavefunction, which is largely confined to the CdSe core.) The idea that EPC is largely influenced by trapped surface charges has been in the literature for a long time and has been invoked to argue that the Huang-Rhys parameters obtained from steady-state resonance Raman data are artificially increased relative to those measured by time-domain techniques.[22, 25] Corroborating support for the idea that hole localization increases EPC comes from our resonance Raman experiments on randomly alloyed CdSe/ZnSe QDs (Figure 3).[3] We found that $Cd_xZn_{1-x}Se$ quantum dots showed much stronger EPC, as inferred from overtone to fundamental intensity ratios, than either pure CdSe or pure ZnSe. CdSe has both a lower conduction band energy and a higher valence band energy than ZnSe, but this effect should be much more important for the holes because of their greater effective mass. Accidental clustering of Cd atoms in a random alloy will tend to localize the holes to regions of the QD, increasing the local electric fields and thereby the EPC (Figure 4). The corresponding effect on Auger recombination rates supports this picture.[46] If trapped surface charges are making the main contribution to localizing the hole wavefunction and amplifying the EPC in single-component QDs, it may be possible to modulate this effect by changing the surface ligands. This is the subject of ongoing work.

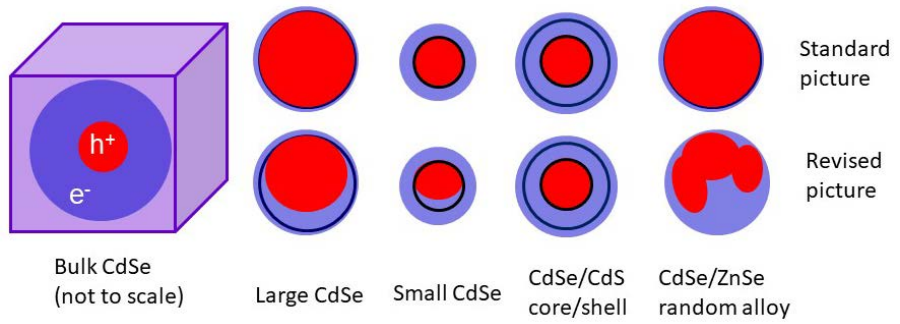

Figure 4. Standard and revised pictures of hole (red) and electron (violet) densities. In the standard picture, bulk CdSe has a large degree of charge separation and therefore large EPC. Reducing the physical size of the crystal first increases the electron-hole overlap and decreases EPC (large CdSe), but then increases EPC because of tunneling of the electron out of the crystal (small CdSe). Adding a CdS shell also extends the electron wavefunction outside the CdSe core and increases EPC for the CdSe phonons. In the revised picture, the hole wavefunction is similarly localized by surface charges in both large and small nanocrystals, producing similar EPC. Adding a CdS shell passivates these charges, allowing the hole wavefunction to spread out and reducing EPC. CdSe/ZnSe random alloys show a much stronger localization of the hole wavefunction by variations in the potential.

There is evidence from other types of experiments that semiconductor nanocrystals in both the wurtzite and zincblende crystal structures have large ground-state dipole moments.[47-48] While a perfect wurtzite crystal should have a dipole moment, a perfect zincblende crystal should not. Experimentally, dipole moments of similar magnitude and size scaling are observed for both crystal structures, suggesting surface charges as a likely mechanism.[47] CdSe QDs with the wurtzite and zincblende structures were also found to have nearly identical resonance Raman intensities, implying very similar EPC.[49] It is plausible that different extents of surface charging are, at least in part, responsible for the large differences in Huang-Rhys parameters obtained for nominally similar systems, and also for the wide range observed for different nanocrystals in single nanocrystal experiments. However, surface charging has yet to be demonstrated as a mechanism for increasing EPC.

Another often neglected aspect of EPC is its dependence on excitonic state. Techniques based on photoluminescence probe the lowest excitonic transition and those within k_BT of it,

but time-domain methods can use pump and probe wavelengths anywhere within the absorption band and resonance Raman spectroscopy is most easily performed with excitation well above the lowest exciton to avoid interfering photoluminescence. Even simple "toy models"[39-40, 50] predict a high density of optically allowed transitions particularly when the different fine-structure spin states are taken into account, and these simple models may underestimate the density of transitions.[51] Combined with the significant inhomogeneous broadening of most nanocrystal absorption spectra, it is generally impossible to probe a single excitonic transition even when exciting near the absorption onset. A few experiments have addressed the excitonic state or excess energy dependence of EPC.[8, 25-26, 44] In particular, our group showed that the so-called "surface optical" phonon in CdSe nanocrystals, which appears as a low-frequency shoulder on the main LO phonon, consists mainly of LO-type phonons with different nodal patterns that couple more effectively to the nodal patterns of the higher-lying excitonic transitions calculated in a particle in a sphere model.[44]

The recent work of Han and Bester may be the first effort to calculate Huang-Rhys parameters or the vibronic structure of the electronic spectrum for II-VI nanocrystals using high-level electronic structure methods.[35] Their calculation on 3.0 nm CdSe QDs (terminated with pseudohydrogen atoms, not real ligands) gives Huang-Rhys parameters distributed over a much larger range of phonon frequencies than is evident in experiments. While different experiments vary greatly on the magnitude of the EPC for this system as summarized in Table 1 and also in Figure S3 of ref. 35, experiments with high enough spectral resolution (resonance Raman and single-particle emission) are in good agreement that nearly all of the EPC in optical modes is limited to a narrow range of frequencies near 205 cm^{-1}. It would be very interesting to see how the Huang-Rhys parameters calculated in ref. 35 vary among similar structures having

slightly different sizes and/or shapes, and whether they are affected by the presence of realistic ligands.

Conclusions and prospects

Exciton-phonon coupling is directly or indirectly related to many of the current and proposed technological applications of semiconductor quantum dots. Furthermore, as it involves both nuclear and electronic degrees of freedom, it is a difficult and worthwhile quantity in which to seek agreement between experiment and theory. There are significant challenges to both the accurate calculation of EPC and its unambiguous experimental measurement, both of which are exacerbated by the poorly defined nature of most semiconductor nanocrystals produced by even the best modern synthetic methods.

Two general types of systems, which are in many ways on opposite ends of the spectrum of semiconductor nanocrystals, appear potentially useful for further exploration. "Magic sized clusters" are very small semiconductor clusters with well-defined stoichiometries and geometries that can be prepared under certain synthetic conditions.[52-55] With the total number of heavy atoms in the dozens compared with hundreds or thousands in more typical nanocrystals, magic sized clusters are far more amenable to high-level electronic structure calculations.[56-59] On the other hand, because their lowest excitonic transitions fall in the blue to uv spectral regions, they are somewhat more difficult to study though the usual optical spectroscopic methods. Also, because of the very high fraction of surface atoms and ligands in such structures, the insights gained from these structures may not be very applicable to larger structures. Studies on magic sized clusters may best be viewed as an arena in which to seek agreement between experiment and theory.

The other nanostructures that may be particularly useful for further exploration are nanoplatelets. The synthetic routes to nanoplatelets produce structures that are very uniform in thickness, leading to narrow absorption and emission spectra. As there is very little quantum confinement in the x and y dimensions, it may be possible for computational purposes to treat them as infinite in these dimensions and take advantage of the methods used for infinite crystals to make the computations tractable.[60-63] A number of quantum chemical calculations have been reported on nanoplatelets[61-63] including calculations of vibrational spectra,[63] but none, to my knowledge, have addressed exciton-phonon coupling. Such studies may also aid in understanding any role of EPC in determining the exciton size in nanoplatelets.[64]

Acknowledgements

This work was supported by NSF grant #CHE-1506803.

References

[1]C. Lin, K. Gong, D. F. Kelley, A. M. Kelley, J. Phys. Chem. C **119**, 7491 (2015).

[2]C. Lin, K. Gong, D. F. Kelley, A. M. Kelley, ACS Nano **9**, 8131 (2015).

[3]K. Gong, D. F. Kelley, A. M. Kelley, J. Phys. Chem. Lett. **8**, 626 (2017).

[4]A. W. Achtstein, A. Schliwa, A. Prudnikau, M. Hardzei, M. V. Artemyev, C. Thomsen, U. Woggon, Nano Lett. **12**, 3151 (2012).

[5]M. J. Fernée, B. N. Littleton, S. Cooper, H. Rubinsztein-Dunlop, D. E. Gomez, P. Mulvaney, J. Phys. Chem. C **112**, 1878 (2008).

[6]E. Groeneveld, C. de Mello Donegá, J. Phys. Chem. C **116**, 16240 (2012).

[7]A. Granados del Aguila, B. Jha, F. Pietra, E. Groeneveld, C. de Mello Donega, J. C. Maan, D. Vanmaekelbergh, P. C. M. Christianen, ACS Nano **8**, 5921 (2014).

[8]J. A. Baker, D. F. Kelley, A. M. Kelley, J. Chem. Phys. **139**, 024702 (2013).

[9]K. Gong, D. F. Kelley, A. M. Kelley, J. Phys. Chem. C **120**, 29533 (2016).

[10]K. Gong, D. F. Kelley, A. M. Kelley, J. Chem. Phys. **147**, 224702 (2017).

[11]A. M. Kelley, J. Phys. Chem. A **117**, 6143 (2013).

[12]A. P. Alivisatos, T. D. Harris, P. J. Carroll, M. L. Steigerwald, L. E. Brus, J. Chem. Phys. **90**, 3463 (1989).

[13]J. J. Shiang, S. H. Risbud, A. P. Alivisatos, J. Chem. Phys. **98**, 8432 (1993).

[14]T. D. Krauss, F. W. Wise, Phys. Rev. B **55**, 9860 (1997).

[15]A. V. Baranov, Y. P. Rakovich, J. F. Donegan, T. S. Perova, R. A. Moore, D. V. Talapin, A. L. Rogach, Y. Masumoto, I. Nabiev, Phys. Rev. B **68**, 165306 (2003).

[16]H. Lange, M. Artemyev, U. Woggon, T. Niermann, C. Thomsen, Phys. Rev. B **77**, 193303 (2008).

[17]H. Lange, M. Mohr, M. Artemyev, U. Woggon, T. Niermann, C. Thomsen, Phys. Stat. Sol. B **247**, 2488 (2010).

[18]B. Zhang, R. Chang, K. Wang, J.-T. Lu, S. Wang, J. Phys. Chem. Lett. **9**, 5055−5062 (2018).

[19]M.-L. Lin, M. Miscuglio, A. Polovitsyn, Y.-C. Leng, B. Martín-García, I. Moreels, P.-H. Tan, R. Krahne, J. Phys. Chem. Lett. **10**, 399−405 (2019).

[20]C. J. A. Maddux, D. F. Kelley, A. M. Kelley, J. Phys. Chem. C **122**, 27100 (2018).

[21]D. M. Mittleman, R. W. Schoenlein, J. J. Shiang, V. L. Colvin, A. P. Alivisatos, C. V. Shank, Phys. Rev. B **49**, 14435 (1994).

[22]F. W. Wise, Acc. Chem. Res. **33**, 773 (2000).

[23]M. R. Salvador, M. W. Graham, G. D. Scholes, J. Chem. Phys. **125**, 184709 (2006).

[24]M. R. Salvador, M. A. Hines, G. D. Scholes, J. Chem. Phys. **118**, 9380 (2003).

[25]D. M. Sagar, R. R. Cooney, S. L. Sewall, E. A. Dias, M. M. Barsan, I. S. Butler, P. Kambhampati, Phys. Rev. B **77**, 235321 (2008).

[26]D. M. Sagar, R. R. Cooney, S. L. Sewall, P. Kambhampati, J. Phys. Chem. C **112**, 9124 (2008).

[27]S. D. Dimitrov, C. J. Dooley, A. A. Trifonov, T. Fiebig, J. Phys. Chem. C **113**, 4198 (2009).

[28]L. J. McKimmie, C. N. Lincoln, J. Jasieniak, T. A. Smith, J. Phys. Chem. C **114**, 82 (2010).

[29]J. Mooney, J. I. Saari, A. M. Kelley, M. M. Krause, B. R. Walsh, P. Kambhampati, J. Phys. Chem. B **117**, 15651 (2013).

[30]T. D. Krauss, F. W. Wise, Phys. Rev. Lett. **79**, 5102 (1997).

[31]A. E. Johnson, A. B. Myers, J. Chem. Phys. **104**, 2497 (1996).

[32]D. Valerini, A. Creti, M. Lomascolo, L. Manna, R. Cingolani, M. Anni, Phys. Rev. B **71**, 235409 (2005).

[33]Z. Sun, I. Swart, C. Delerue, D. Vanmaekelbergh, P. Liljeroth, Phys. Rev. Lett. **102**, 196401 (2009).

[34]H. Wang, E. Lhuillier, Q. Yu, A. Mottaghizadeh, C. Ulysse, A. Zimmers, A. Descamps-Mandine, B. Dubertret, H. Aubin, Phys. Rev. B **92**, 041403(R) (2015).

[35]P. Han, G. Bester, Phys. Rev. B **99**, 100302(R) (2019).

[36]A. M. Kelley, ACS Nano **5**, 5254 (2011).

[37]A. M. Kelley, J. Chem. Phys. **144**, 214702 (2016).

[38]P. Han, G. Bester, Phys. Rev. B **96**, 195436 (2017).

[39]A. L. Efros, M. Rosen, M. Kuno, M. Nirmal, D. J. Norris, M. Bawendi, Phys. Rev. B **54**, 4843 (1996).

[40]D. J. Norris, A. L. Efros, M. Rosen, M. G. Bawendi, Phys. Rev. B **53**, 16347 (1996).

[41]M. Shim, P. Guyot-Sionnest, Phys. Rev. B **64**, 245342 (2001).

[42]J. L. Blackburn, H. Chappell, J. M. Luther, A. J. Nozik, J. C. Johnson, J. Phys. Chem. Lett. **2**, 599 (2011).

[43]J. Habinshuti, O. Kilian, O. Cristini-Robbe, A. Sashchiuk, A. Addad, S. Turrell, E. Lifshitz, B. Grandidier, L. Wirtz, Phys. Rev. B **88**, 115313 (2013).

[44]C. Lin, D. F. Kelley, M. Rico, A. M. Kelley, ACS Nano **8**, 3928 (2014).

[45]D. S. Egolf, M. R. Waterland, A. M. Kelley, J. Phys. Chem. B **104**, 10727 (2000).

[46]D. Morgan, K. Gong, A. M. Kelley, D. F. Kelley, J. Phys. Chem. C **121**, 18307 (2017).

[47]M. Shim, P. Guyot-Sionnest, J. Chem. Phys. **111**, 6955 (1999).

[48]S. A. Blanton, R. L. Leheny, M. A. Hines, P. Guyot-Sionnest, Phys. Rev. Lett. **79**, 865 (1997).

[49]A. M. Kelley, Q. Dai, Z. Jiang, J. A. Baker, D. F. Kelley, Chem. Phys. **422**, 272 (2013).

[50]A. I. Ekimov, F. Hache, M. C. Schanne-Klein, D. Ricard, C. Flytzanis, I. A. Kudryavtsev, T. V. Yazeva, A. V. Rodina, J. Opt. Soc. Am. B **10**, 100 (1993).

[51]L.-W. Wang, A. Zunger, J. Phys. Chem. B **102**, 6449 (1998).

[52]V. N. Soloviev, A. Eichhofer, D. Fenske, U. Banin, J. Am. Chem. Soc. **123**, 2354 (2001).

[53]N. Herron, J. C. Calabrese, W. E. Farneth, Y. Wang, Science **259**, 1426 (1993).

[54]A. N. Beecher, X. Yang, J. H. Palmer, A. L. LaGrassa, P. Juhas, S. J. L. Billinge, J. S. Owen, J. Am. Chem. Soc. **136**, 10645−10653 (2014).

[55]S. M. Harrell, J. R. McBride, S. J. Rosenthal, Chem. Mater. **8**, 1199 (2013).

[56]K. A. Nguyen, R. Pachter, P. N. Day, J. Phys. Chem. A **121**, 1748−1759 (2017).

[57]K. A. Nguyen, R. Pachter, J. Jiang, P. N. Day, J. Phys. Chem. A **122**, 6704−6712 (2018).

[58]X. Zhu, G. A. Chass, L.-C. Kwek, A. L. Rogach, H. Su, J. Phys. Chem. C **119**, 29171−29177 (2015).

[59]M. Del Ben, R. W. A. Havenith, R. Broer, M. Stener, J. Phys. Chem. C **115**, 16782 (2011).

[60]S. Pal, P. Nijjar, T. Frauenheim, O. V. Prezhdo, Nano Lett. **17**, 2389−2396 (2017).

[61]A. Szemjonov, T. Pauporte, S. Ithurria, N. Lequeux, B. Dubertret, I. Ciofini, F. Labat, RSC Adv. **4**, 55980 (2014).

[62]R. S. Koster, C. Fang, A. van Blaaderen, M. Dijkstraa, M. A. van Huis, Phys. Chem. Chem. Phys. **18**, 22021 (2016).

[63]A. Szemjonov, T. Pauporte, S. I. Ithurria, B. Dubertret, I. Ciofini, F. Labat, Langmuir **34**, 13828−13836 (2018).

[64]D. P. Morgan, D. F. Kelley, J. Phys. Chem. C **123**, 18665 (2019).